The heterogeneous photo-Fenton reaction using goethite as catalyst

Guadalupe B. Ortiz de la Plata, Orlando M. Alfano and Alberto E. Cassano

ABSTRACT

In the present work the degradation of 2-chlorophenol (2-CP) used as model compound, applying the Heterogeneous photo-Fenton reaction, was studied. Small particles of goethite or iron oxyhydroxide were used as a source of iron. The influence of catalyst loading, radiation intensity and the molar ratio between hydrogen peroxide and contaminant were examined. Improvement by illumination is highly significant. During the progress of 2-CP degradation, the reaction shows an unusual acceleration. This autocatalytic comportment, with stronger tendencies at higher temperatures, implies a completely different behaviour from the one typically expected. The autocatalytic performance is successfully explained by the joint action of two factors: (i) the evolution of the available iron in the homogeneous phase during the course of the reaction and (ii) the autocatalytic contribution of some of the reaction intermediates in the iron cycle. The small iron concentration leaching into the solution is produced by two typical liquid medium – solid goethite surface dissolution processes. A reaction mechanism has been proposed and, in a first stage, parameters have been obtained for the dark reaction. In a second step, the complete data for the irradiated operation were obtained.

Key words | 2-chlorophenol, Fenton, goethite, heterogeneous, radiation enhancement

Guadalupe B. Ortiz de la Plata
Orlando M. Alfano (corresponding author)
Alberto E. Cassano
INTEC, CONICET and Universidad Nacional del Litoral,
Güemes 3450,
3000 Santa Fe,
Argentina
E-mail: *guadaortiz@santafe-conicet.gov.ar*; *alfano@santafe-conicet.gov.ar*; *acassano@santafe-conicet.gov.ar*

INTRODUCTION

The Fenton reaction has been known for many years; it provides a useful tool for pollutant degradation (Fenton 1894) and has often been used in many applications. It can be enhanced by increasing the temperature or application of UV-Visible radiation (the photo-Fenton reaction). These two improvements can be achieved simultaneously employing solar irradiation. The process is usually conducted at pH 3 to maintain the iron compound in solution and requires a down-stream treatment to raise the pH and settle the catalyst. This separation is not simple for the particular colloidal characteristics of the resulting dispersion.

In the last years, it has been suggested to use immobilised iron containing compounds in many different forms to overcome this problem. This technology, known as Heterogeneous Fenton, uses hydrogen peroxide (H_2O_2) and a solid iron carrier to facilitate iron separation, employing mainly solid supporters to avoid more complex post treatment processes (Feng *et al.* 2004; Pignatello *et al.* 2006; Ortiz de la Plata *et al.* 2008). This technology employs a variety of methods to incorporate iron to the system, resorting to either different supports to immobilise the solid or compact iron aggregations such as different forms of iron oxides. Among the compounds that have been examined can be mentioned: membranes (Fernandez *et al.* 1998), alginates (Fernandez *et al.* 2000), silica (Bozzi *et al.* 2004; Huang & Huang 2008), zeolites (Neamtu *et al.* 2004; Zheng *et al.* 2004), clays like bentonites and laponites (Feng *et al.* 2005, 2009; Garrido-Ramirez *et al.* 2010), alumina (Cuzzola *et al.* 2002), glass (Martínez *et al.* 2007), and activated carbon (Yuranova *et al.* 2004). The second option includes synthesised as well as natively found iron oxides (Chou *et al.* 2001; Huang *et al.* 2001; Cuzzola *et al.* 2002; Lu *et al.* 2002;

doi: 10.2166/wst.2010.258

Feng *et al.* 2004; Teel *et al.* 2007; Huang & Huang 2008) and, most recently, particles of solid zero valent iron (Liao *et al.* 2003; Bergendahl & Thies 2004; Devi *et al.* 2009; Morgada *et al.* 2009; Son *et al.* 2009). Among the iron oxides, goethite (Lin & Gurol 1998; Gurol & Lin 2001; Lu *et al.* 2002; Lin & Lu 2007; Gordon & Marsh 2009; Garrido-Ramirez *et al.* 2010) seems to be a reasonable choice because it combines three attractive properties for large-scale applications; among others stand out (Ortiz de la Plata *et al.* 2008): (i) wide range of operating pH, (ii) controllable leaching of iron into the solution and (iii) the possibility of using solar radiation as a primary source of energy for a photo-Fenton alternative.

2-Chlorophenol (2-CP) is used as germicide/disinfectant and as precursor for synthesising pesticides and other chlorophenols. It can also be produced as a byproduct in water disinfection and in pulp bleaching (*Toxicological Profile for Chlorophenols* 1999).

In the present work the degradation of 2-CP as model compound was studied and goethite iron oxyhydroxide was used as a source of iron. The influence of catalyst loading, UVA radiation intensity and the molar ratio of hydrogen peroxide to contaminant was examined.

METHODS

Materials

Goethite was provided by Aldrich (catalytic grade); originally, they were particles of 30–50 mesh (297 to 600 μm), from which the segment of 75–150 μm was used. A complete and detailed description of the catalyst can be seen in other works of the authors (Ortiz de la Plata *et al.* 2008, 2010). 2-CP was provided by Aldrich 99% + . Hydrogen peroxide (H_2O_2) was provided by Cicarelli (ACS, 30%). Finally, chlorobenzoquinone (ClBQ) 95% + and chlorohydroquinone (ClHQ) 85% + were provided by Aldrich. pH was adjusted with perchloric acid (ByA, ACS, 70%).

Photo-Fenton experimental device and procedures

The work was performed in a cylindrical, well-stirred, batch reactor irradiated from a transparent radiation bottom, which was illuminated with a tubular lamp placed at the focal axis of a parabolic reflector (Figure 1 and Table 1). The reactor was also equipped with internal glass heat exchangers connected to a thermostatic bath for controlling temperature and an external insulation made of K-Wool. The described device allows irradiating the suspension with photons whose wavelength range goes from 340 to 380 nm.

The reactor was filled with pure water and the desired concentration of goethite. Then, 2-CP was added to reach an initial concentration of 0.39 mM (50 ppm). After reaching steady-state temperature (and, when corresponds, lamp irradiation), the prescribed H_2O_2 was incorporated to the system. pH was adjusted with perchloric acid. The range of the initial molar ratio of $C_{H_2O_2,0}$ to $C_{2\text{-CP},0}$ (R) was varied from 0 to 50 (four levels); the catalyst loading was varied in four levels from 0 to 2 g L^{-1} and the temperature was set at 25°C. Irradiation was varied in three levels, 0, 48 and 100% referred to the maximum power input. All of them were measured by actinometry (see Table 1).

Blank runs were made to exclude other parallel reaction mechanisms. Direct photolysis and/or direct H_2O_2 oxidation were safely disregarded. Variations in 2-CP concentrations were less than 2% with no definite tendencies along 6 h of experiments with and without irradiation.

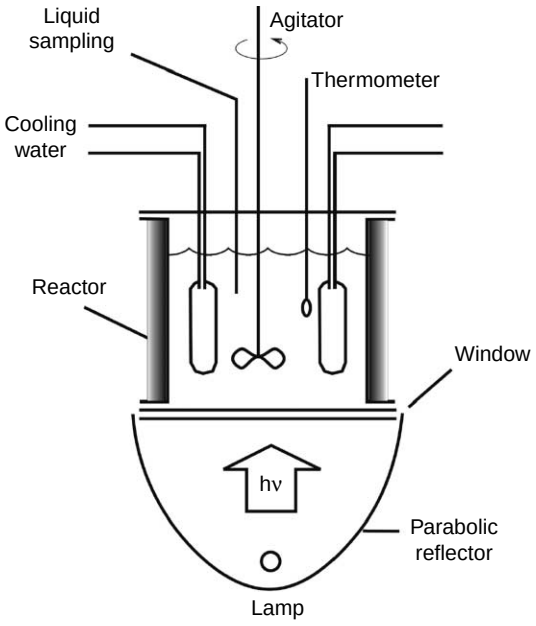

Figure 1 | Schematic representation of the experimental reactor.

Table 1 | Characteristics of the experimental reactor

Main characteristic dimension	Operating depth = 9 cm
Reactor inner diameter	17 cm
Reactor volume	2,000 cm^3
Reactor bottom made of	Acrylic/borosilicate glass
Lamp (one)	Tubular, located at the focal axis of a parabolic reflector
Lamp type	Phillips TL'D 18W/08
Nominal input power	18 W
Emission range of the lamp	$\lambda = 340-420$ nm
Lamp diameter	2.6 cm
Lamp length	59 cm
Reflector	Parabolic cylinder
Incident radiation at the reactor bottom (100%)	5.60×10^{-9} Einstein s^{-1} cm^{-2}

Running 2-CP with the maximum goethite loading (2 g L^{-1}), no changes were found in concentrations before and after the addition of the catalyst. It has been shown that there is no loss of pollutant by adsorption (Ortiz de la Plata *et al.* 2010).

Analytical methods

2-CP, ClBQ and ClHQ concentrations were monitored with HPLC (Waters) equipped with a LC-18 Supelcosil reversed-phase column. The eluent was a ternary mixture of water (containing 1% v/v acetic acid), methanol, and acetonitrile (60:30:10), pumped at a rate of 1 mL min^{-1}. UV detection of 2-CP and ClHQ was performed at 280 nm while ClBQ was measured at 254 nm. Reaction intermediates have been identified by GC-MS. A portion of sample was placed in a vial of 10 mL capacity for performing a solid-phase micro-extraction in a headspace, SPME/HS (Pawliszyn 1999). The extract was then analysed by gas chromatography with mass spectrometer detector (GC/MS) Varian Saturn 2000, which has a database of mass spectra references NIST. The identification of compounds was performed by comparison with the information in the database. Total organic carbon (TOC) was measured with a Shimadzu TOC-5000 Analyser. H_2O_2 was measured spectrophotometrically with a modified iodometric technique (Allen *et al.* 1952); ferrous ions were analysed spectrophotometrically by means of absorbance of the Fe^{2+}-phenanthroline complex at 510 nm (*Standard Methods* 1995). A Cary 100 Bio spectrophotometer was used for both analyses. Finally, total dissolved iron content was measured using ascorbic acid as a reducing agent. Total iron content in the solution was measured by AAS (Perkin Elmer A Analyst 800). Before analysis, solid particles were separated by filtration with Whatman Syringe filters of 0.02 μm.

RESULTS AND DISCUSSION

Experimental results

Experimentally the appearance of two intermediaries is clearly observed: Cl-benzoquinone (ClBQ), which has been identified together with Cl-hydroquinone (ClHQ) by GC-MS from reaction samples. During the progress of the degradation of 2-CP, the reaction shows an unusual acceleration. This autocatalytic behaviour, with stronger tendencies at higher temperatures (not shown here), implies a completely different behaviour from the one typically expected. Improvement employing radiation is very significant (Table 2 and Figure 2).

Table 2 | Reaction conditions and percent conversion of 2-CP, TOC and H_2O_2 after 6 h of reaction

	C_{Cat} (g L^{-1})	R	% Rad	$X_{2\text{-}CP}$ (%)	X_{TOC} (%)	$X_{H_2O_2}$(%)
R1F	2	50	0	19.1	10.0	94.7
R2F	2	30	0	7.9	5.7	97.9
R3F	0.5	50	0	7.3	6.9	47.4
R4F	0.5	30	0	5.9	3.4	53.1
R5F	1.25	37	0	12.0	9.0	83.6
R6F	1.25	40	0	12.4	9.0	82.4
R1PF	2	50	100	88.51	73.1	90.6
R2PF	2	30	100	62.71	46.43	95.62
R3PF	0.5	50	100	41.5	21.08	43.01
R4PF	0.5	30	100	41.44	20.03	45
R5PF	1.25	40	48	53.95	37.67	83.15
R6PF	1.25	26	100	86.63	59.95	84.42
R7PF	1.25	40	100	88.65	58.51	79.74
R8PF	1.25	40	48	52.1	33.5	81.45

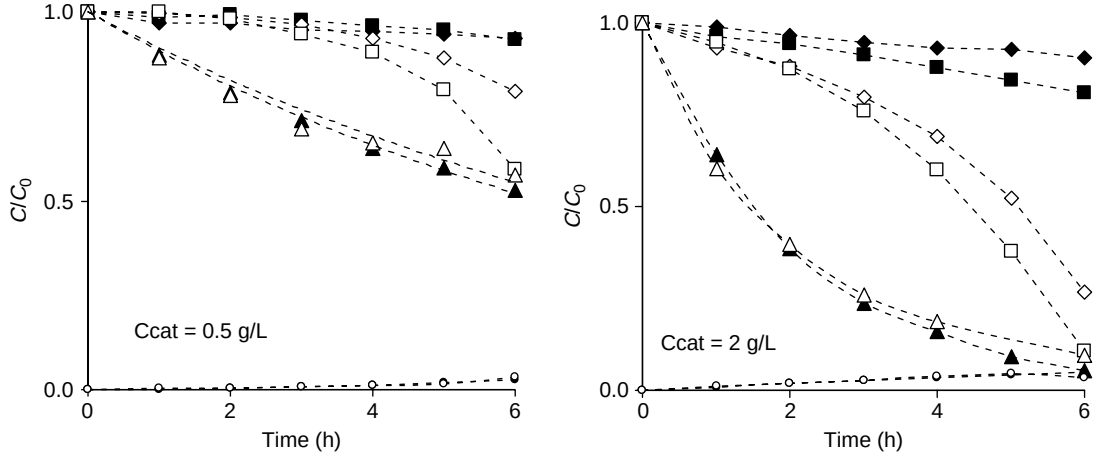

Figure 2 | Experimental results for $R \cong 50$. References: ◆, ◇: TOC/TOC$_0$; ■, □: $C_{2\text{-CP}}/C_{2\text{-CP},0}$; ▲, △: $C_{H_2O_2}/C_{H_2O_2,0}$; ●, ○: $C_{ClBQ}/C_{2\text{-CP},0}$. Black: Fenton; white: photo Fenton.

Proposed reaction mechanism

The autocatalytic performance is successfully explained by the joint action of two factors: the evolution of the available iron in the homogeneous phase during the course of the reaction (Lin & Lu 2007), and the autocatalytic contribution of some of the reaction intermediaries in the iron cycle (Chen & Pignatello 1997). A reaction mechanism has been proposed (Ortiz de la Plata *et al.* 2010). Table 3 depicts the proposed reaction scheme.

The classical Fenton reaction improvement obtained by applying radiation is due to Reaction (20). Additionally, Chen & Pignatello (1997) established for phenolic compounds the existence of a benzoquinone photochemical reaction occurring in the wavelength range from 300 to 480 nm. The high differences observed in conversions between the Fenton and photo-Fenton reactions are parallel to the appearance of higher concentrations of ClHQ (resulting from an additional photochemical step) and a correlatively low increasing rate in the relative amount of ClBQ. This behaviour is explained as follows. The above mentioned ClBQ–ClHQ intervention in the iron leaching processes is complemented with the development of an additional photochemical step (Reaction (21)) that leads to the formation of ClSQ· and OH· radicals that contribute to the enhancement of the overall reaction efficiency.

The rate expressions for reactions (20) and (21) are given by $r_{Fe(OH)^{2+}} = \Phi_{Fe(OH)^{2+}} e^a_{Fe(OH)^{2+}}$ and $r_{ClBQ} = \Phi_{ClBQ} e^a_{ClBQ}$ respectively, where Φ_i represents the quantum yield for each reaction. Consequently, it will become necessary to calculate two local volumetric photon absorption rates ($e^a_{Fe(OH)^{2+}}$ and e^a_{ClBQ}), one for each photoreaction. It must be noticed that both are based on the solution of a unique radiation balance.

Radiation model

The knowledge of the radiation field necessary to compute each e^a was obtained by solving the radiative transfer Equation (RTE) for the heterogeneous system, applying a one-dimensional–one-directional radiation transport model, that employs diffuse irradiation (producing azimuthal symmetry). It was deduced from a particular case of the general RTE (Ozisik 1973; Cassano *et al.* 1995) by (Alfano *et al.* 1997):

$$\mu \frac{dI_{\lambda,\theta}(x,\mu,t)}{dx} + \underbrace{\kappa_{\lambda,T}(t) I_{\lambda,\theta}(x,\mu,t)}_{\text{absorption}} + \underbrace{\sigma_{\lambda,T}(t) I_{\lambda,\theta}(x,\mu,t)}_{\text{scattering out}}$$

$$= \underbrace{\frac{\sigma_{\lambda,T}(t)}{2} \int_{\mu'=1}^{1} I_{\lambda,\theta}(x,\mu',t) p(\mu,\mu') d\mu'}_{\text{scattering in}} \quad (1)$$

where λ represents the radiation wavelength; I_λ is the spectral Radiation Intensity (Einstein cm^{-2}S^{-1}rad^{-1}); x, the axial coordinate (cm); $\mu = \cos\theta$, the direction cosine of the ray for which the RTE is written; μ', the cosine of the

Table 3 | Reaction mechanism

	Reactions	Constants	Values
1	$Fe^{3+} + H_2O_2 \rightarrow Fe^{2+} + H^+ + HO_2^{\cdot}$	k_1	1.91×10^{-2}
2	$Fe^{2+} + H_2O_2 \rightarrow Fe^{3+} + HO^- + HO^{\cdot}$	k_2	5.21×10^{1}
3	$H_2O_2 + HO^{\cdot} \rightarrow HO_2^{\cdot} + H_2O$	k_3	2.70×10^{7}
4	$H_2O_2 + HO_2^{\cdot} \rightarrow HO^{\cdot} + H_2O + O_2$	k_4	3.00
5	$Fe^{3+} + HO_2^{\cdot} \rightarrow Fe^{2+} + H^+ + O_2$	k_5	1.00×10^{4}
6	$Fe^{2+} + HO_2^{\cdot} + H^+ \rightarrow Fe^{3+} + H_2O_2$	k_6	1.20×10^{6}
7	$Fe^{2+} + HO^{\cdot} \rightarrow Fe^{3+} + HO^-$	k_7	3.20×10^{8}
8	$HO^{\cdot} + 2 - CP \rightarrow ClDHCD^{\cdot}$	k_8	1.29×10^{9}
9	$Fe^{3+} + ClDHCD^{\cdot} \rightarrow Fe^{2+} + ClHQ$	k_9	6.60×10^{3}
10	$Fe^{3+} + ClHQ \rightarrow Fe^{2+} + ClSQ^{\cdot}$	k_{10}	4.38×10^{2}
11	$Fe^{3+} + ClSQ^{\cdot} \rightarrow Fe^{2+} + ClBQ$	k_{11}	4.40×10^{4}
12	$HO^{\cdot} + ClBQ \rightarrow$ Products	k_{12}	1.20×10^{9}
13	$HO^{\cdot} + ClDHCD^{\cdot} \rightarrow$ Products	k_{13}	2.00×10^{10}
14	$ClDHCD^{\cdot} + O_2 \rightarrow ClHQ + HO_2^{\cdot}$	k_{14}	6.00×10^{9}
15	$ClDHCD^{\cdot} + O_2 \rightarrow$ Products	k_{15}	4.00×10^{9}
16	$HO^{\cdot} + ClHQ \rightarrow$ Products	k_{16}	7.00×10^{9}
17	$H_2O_2 \xrightarrow{\alpha-FeOOH} \frac{1}{2}O_2 + H_2O$	k_{17}	6.75×10^{-5}
18	$\alpha - FeOOH + 3H^+ \rightarrow Fe^{3+} + 2H_2O +$ site	k_{18}	5.23×10^{-11}
19	$2\alpha - FeOOH + ClHQ \rightarrow 2Fe^{2+} + ClBQ + 4OH^-$	k_{19}	2.41×10^{-6}
20	$Fe^{III}(OH)^{2+} \xrightarrow{h\nu} Fe^{2+} + HO^{\cdot}$	$\Phi_{Fe(OH)^{2+}}$	2.67×10^{-1}
21	$ClBQ \xrightarrow{h\nu} ClSQ^{\cdot} + HO^{\cdot}$	Φ_{ClBQ}	6.84×10^{-1}

Constants 1 to 7 and 9 to 16 from literature (Chen & Pignatello 1997; Kang *et al.* 2002; Ma *et al.* 2005). Units in $M^{-1}s^{-1}$, except k_{17} ($L\,g^{-1}\,s^{-1}$) and k_{18} ($mol\,g^{-1}\,s^{-1}$). For reactions (14) and (15), 0.25×10^{-3} M oxygen concentration was considered.

incident ray before scattering; and p represents the phase function for scattering. The solution of this equation provides the values of the spectral Radiation Intensities as a function of position and direction for each wavelength.

To calculate the photons absorbed by the absorbing species in any photo-initiated reaction it is first necessary to calculate the radiation reaching that point. In the more general case, and even more in a scattering medium, the radiation may come from all spatial directions. The integration of the spectral Specific Intensity in all directions is defined as the spectral Incident Radiation, G_λ. In the case of a one-dimensional distribution of radiation directions due to the previously mentioned azimuthal symmetry, G_λ can be simplified to:

$$G_\lambda = 2\pi \int_{\mu=-1}^{\mu=1} I_\lambda(x, \mu) \mathrm{d}\mu \tag{2}$$

The radiant energy absorbed by a specific radiation absorbing species, "j", on an elementary volume is defined as the spectral and total local volumetric rate of photon absorption respectively ($e^a_{\lambda,j}$ and e^a_j). The spectral local volumetric rate of photon absorption is:

$$e^a_{\lambda,j}(x) = \kappa_{\lambda,j} G_\lambda(x, \kappa_{\lambda,T}, \sigma_{\lambda,\mathrm{Goet}}) \tag{3}$$

$$\kappa_{\lambda,T} = \sum_{i=1}^{N} \kappa_{\lambda,i} \tag{4}$$

Equations (3) and (4) show the case of a medium where there are N radiation absorbing species and one, "j", is particularly considered to calculate its local volumetric rate of photon absorption.

In this case, there are three different radiation absorbing species: however, only one also scatters. Thus, the absorption coefficient of the medium is given by:

$$\begin{aligned}\kappa_{\lambda,T}(t) &= \kappa_{\lambda,\mathrm{Goet}} + \kappa_{\lambda,Fe(OH)^{2+}}(t) + \kappa_{\lambda,\mathrm{ClBQ}}(t) \\ &= \kappa^*_{\lambda,\mathrm{Goet}} C_{\mathrm{Cat}} + \kappa^*_{\lambda,Fe(OH)^{2+}} C_{Fe(OH)^{2+}}(t) + \kappa^*_{\lambda,\mathrm{ClBQ}} \\ &\quad C_{\mathrm{ClBQ}}(t)\end{aligned} \tag{5}$$

In addition, the scattering coefficient:

$$\sigma_{\lambda,T} = \sigma_{\lambda,\mathrm{Goet}} = \sigma^*_{\lambda,\mathrm{Goet}} C_{\mathrm{Cat}} \tag{6}$$

The Discrete Ordinate Method (Duderstadt & Martin 1979) was applied to solve the RTE. Isotropic (diffuse) boundary condition for the bottom of the reactor and no reflections from the top were applied. The solution of the RTE provides the Radiation Intensity at each point and each direction inside the reactor. Because concentrations of homogeneous species evolve over the time of reaction, it is necessary to solve the differential mass balance as a function of time, coupled with the RTE through their concentration dependencies that change during the progress of the reaction.

Optimisation procedure

The values of the constants that are not available in the literature were obtained using an adapted nonlinear,

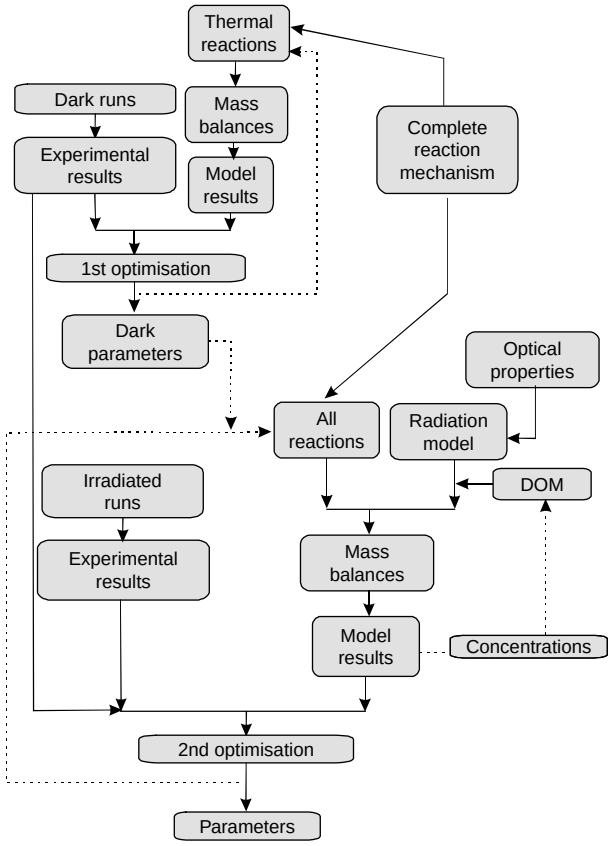

Figure 3 | Schematic representation of the sequential algorithm employed for parameters optimisation.

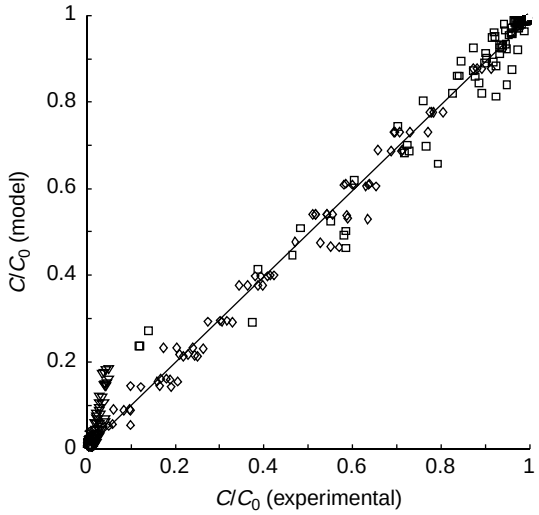

Figure 4 | Dimensionless experimental concentrations vs. model simulation results. Symbols: □ $C_{2\text{-CP}}/C_{2\text{-CP},0}$, ◇ $C_{H_2O_2}/C_{H_2O_2,0}$, ▽ $C_{ClBQ}/C_{2\text{-CP},0}$ and ◁ $C_{ClHQ}/C_{2\text{-CP},0}$.

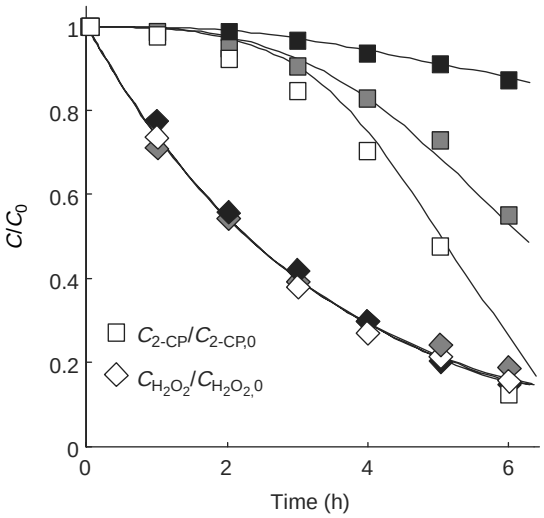

Figure 5 | Dimensionless experimental results and model simulations vs. time. Black: Fenton 0% irrad; grey: photo-Fenton 48% irrad.; white: photo-Fenton 100% irradiation (dark). Solid lines are model simulations.

multiparameter optimisation program (Levenberg-Marquardt). The concentration values of the model simulations were compared with those obtained from experiments for the following compounds: 2-CP, H_2O_2, ClHQ and ClBQ in order to obtain the unknown kinetic constants.

Due to the low concentration of iron observed in dark reactions (close to the limit of detection) it was necessary to resort to a compromising decision. In a first step, the dissolution process was restricted to a single stage of leaching (the proton promoted dissolution represented by Reaction (18)). This step limited the increase in the iron content to a value that was set equal to the maximum amount of dissolved iron observed in the dark runs (0.15 ppm) and used to calculate the kinetic constants of the Heterogeneous Fenton reaction. In a second stage, the constant for the reductive dissolution of iron by quinones (Reaction (19)) was obtained when the concentration of iron observed in the irradiated runs reached higher values (0.3 ppm) without entering into conflict with the detection limit of the analytical method (AAS). Due to the low amount of dissolved iron observed in both conditions and the high levels of H_2O_2 present in the reaction medium, it was not possible to differentiate the iron species accurately. Thus, iron speciation was simulated by the model. Figure 3 shows the complete calculation procedure employed to evaluate the rate constants that were not known.

Figure 4 shows a good agreement between simulation results with the experimental values for the four most important reacting species. Figure 5 shows the results of the optimisation. It can be seen that the agreement is very satisfactory. In addition, it shows that the adjustment of the dark Heterogeneous Fenton reaction remains very adequate after taking into account the ClHQ reductive leaching.

CONCLUSIONS

A complete reaction scheme and a kinetic model have been developed that satisfactorily describe both the homogeneous and heterogeneous reactions coexisting in the process. It also gives very good agreement for each one of the possible operating conditions: (i) operation employing radiation (the Heterogeneous photo-Fenton reaction) and (ii) dark operation; i.e., the thermal Heterogeneous Fenton process. Under isothermal conditions at 25°C, when comparing the values of conversion of 2-CP and TOC under different operating conditions, it is possible to conclude that: 1) higher catalyst loading and 2) larger hydrogen peroxide to 2-CP concentration ratios always implies higher conversions. Light improvement is remarkably significant. Under the same operating conditions, applying radiation, the efficiency is increased, on the average, approximately one order of magnitude. Iron leaching into the reacting solution is extremely low. It allows the direct release of the process outcome without further treatment, complying with the iron concentration limits set by the European Union. Moreover, if the remaining hydrogen peroxide becomes undesirable, it can be readily eliminated by simple superficial degradation produced by the goethite particles.

REFERENCES

Alfano, O. M., Cabrera, M. I. & Cassano, A. E. 1997 Photocatalytic reactions involving hydroxyl radical attack: I. Reaction kinetics formulation with explicit photon absorption effects. *J. Catal.* **172**(2), 370–379.

Allen, A. O., Hochanadel, C. J., Ghormley, J. A. & Davis, T. W. 1952 Decomposition of water and aqueous solutions under mixed fast neutron and gamma radiation. *J. Phys. Chem.* **56**(5), 575–586.

Bergendahl, J. A. & Thies, T. P. 2004 Fenton's oxidation of MTBE with zero-valent iron. *Water Res.* **38**(2), 327–334.

Bozzi, A., Yuranova, T., Mielczarski, J. & Kiwi, J. 2004 Evidence for immobilized photo-Fenton degradation of organic compounds on structured silica surfaces involving Fe recycling. *New J. Chem.* **28**(4), 519–526.

Cassano, A. E., Martin, C. A., Brandi, R. J. & Alfano, O. M. 1995 Photoreactor analysis and design: fundamentals and applications. *Ind. Eng. Chem. Res.* **34**(7), 2155–2201.

Chen, R. & Pignatello, J. J. 1997 Role of quinone intermediates as electron shuttles in Fenton and photoassisted Fenton oxidations of aromatic compounds. *Environ. Sci. Technol.* **31**(8), 2399–2406.

Chou, S., Huang, C. & Huang, Y. H. 2001 Heterogeneous and homogeneous catalytic oxidation by supported α-FeOOH in a fluidized-bed reactor: kinetic approach. *Environ. Sci. Technol.* **35**(6), 1247–1251.

Cuzzola, A., Bernini, M. & Salvadori, P. 2002 A preliminary study on iron species as heterogeneous catalysts for the degradation of linear alkylbenzene sulphonic acids by H_2O_2. *Appl. Catal. B Environ.* **36**(3), 231–237.

Devi, L. G., Girish Kumar, S., Mohan Reddy, K. & Munikrishnappa, C. 2009 Photo degradation of methyl orange an azo dye by advanced Fenton process using zero valent metallic iron: Influence of various reaction parameters and its degradation mechanism. *J. Hazard. Mater.* **164**(2–3), 459–467.

Duderstadt, J. J. & Martin, R. 1979 *Transport Theory*. Wiley, New York.

Feng, J., Hu, X. & Yue, P. L. 2004 Discoloration and mineralization of orange II using different heterogeneous catalysts containing Fe: a comparative study. *Environ. Sci. Technol.* **38**(21), 5773–5778.

Feng, J., Hu, X. & Yue, P. L. 2005 Discoloration and mineralization of orange II by using a bentonite clay-based Fe nanocomposite film as a heterogeneous photo-Fenton catalyst. *Water Res.* **39**(1), 89–96.

Feng, J., Hu, X., Yue, P. L. & Qiao, S. 2009 Photo Fenton degradation of high concentration orange II (2 mM) using catalysts containing Fe: a comparative study. *Sep. Purif. Technol.* **67**(2), 213–217.

Fenton, H. J. H. 1894 Oxidation of tartaric acid in presence of iron. *J. Chem. Soc. Trans.* **65**, 899–911.

Fernandez, J., Bandara, J., Lopez, A., Albers, P. & Kiwi, J. 1998 Efficient photo-assisted Fenton catalysis mediated by Fe ions on Nafion membranes active in the abatement of non-biodegradable azo-dye. *Chem. Commun.* **14**, 1493–1494.

Fernandez, J., Dhananjeyan, M. R., Kiwi, J., Senuma, Y. & Hilborn, J. 2000 Evidence for Fenton photoassisted processes mediated by encapsulated Fe ions at biocompatible pH values. *J. Phys. Chem. B* **104**(22), 5298–5301.

Garrido-Ramirez, E. G., Theng, B. K. G. & Mora, M. L. 2010 Clays and oxide minerals as catalysts and nanocatalysts in Fenton-like reactions–a review. *Appl. Clay Sci.* **47**(3–4), 182–192.

Gordon, T. R. & Marsh, A. L. 2009 Temperature dependence of the oxidation of 2-chlorophenol by hydrogen peroxide in the Presence of goethite. *Catal. Lett.* **132**(3–4), 349–354.

Gurol, M. D. & Lin, S. S. 2001 Hydrogen peroxide/iron oxide-induced catalytic oxidation of organic compounds. *Water Sci. Technol. Water Supply* **1**(4), 131–138.

Huang, C. P. & Huang, Y. H. 2008 Comparison of catalytic decomposition of hydrogen peroxide and catalytic degradation of phenol by immobilized iron oxides. *Appl. Catal. A Gen.* **346**(1–2), 140–148.

Huang, H. H., Lu, M. C. & Chen, J. N. 2001 Catalytic decomposition of hydrogen peroxide and 2-chlorophenol with iron oxides. *Water Res.* **35**(9), 2291–2299.

Kang, N., Lee, D. S. & Yoon, J. 2002 Kinetic modeling of Fenton oxidation of phenol and monochlorophenols. *Chemosphere* **47**(9), 915–924.

Liao, C. H., Kang, S. F. & Hsu, Y. W. 2003 Zero-valent iron reduction of nitrate in the presence of ultraviolet light, organic matter and hydrogen peroxide. *Water Res.* **37**(17), 4109–4118.

Lin, S. S. & Gurol, M. D. 1998 Catalytic decomposition of hydrogen peroxide on iron oxide: kinetics, mechanism, and implications. *Environ. Sci. Technol.* **32**(10), 1417–1423.

Lin, Y. T. & Lu, M. C. 2007 Catalytic action of goethite in the oxidation of 2-chlorophenols with hydrogen peroxide. *Water Sci. Technol.* **55**(12), 101–106.

Lu, M. C., Chen, J. N. & Huang, H. H. 2002 Role of goethite dissolution in the oxidation of 2-chlorophenol with hydrogen peroxide. *Chemosphere* **46**(1), 131–136.

Ma, J., Song, W., Chen, C., Cheng, M., Ma, W., Zhao, J. & Tang, Y. 2005 Fenton degradation of organic compounds promoted by dyes under visible irradiation. *Environ. Sci. Technol.* **39**(15), 5810–5815.

Martínez, F., Calleja, G., Melero, J. A. & Molina, R. 2007 Iron species incorporated over different silica supports for the heterogeneous photo-Fenton oxidation of phenol. *Appl Catal. B Environ.* **70**(1–4), 452–460.

Morgada, M. E., Levy, I. K., Salomone, V., Farías, S. S., López, G. & Litter, M. I. 2009 Arsenic (V) removal with nanoparticulate zerovalent iron: effect of UV light and humic acids. *Catal. Today* **143**(3–4), 261–268.

Neamtu, M., Zaharia, C., Catrinescu, C., Yediler, A., Macoveanu, M. & Kettrup, A. 2004 Fe-exchanged Y zeolite as catalyst for wet peroxide oxidation of reactive azo dye Procion Marine H-EXL. *Appl. Catal. B Environ.* **48**(4), 287–294.

Ortiz de la Plata, G. B., Alfano, O. M. & Cassano, A. E. 2008 Optical properties of goethite catalyst for heterogeneous photo-Fenton reactions: Comparison with a titanium dioxide catalyst. *Chem. Eng. J.* **137**(2), 396–410.

Ortiz de la Plata, G. B., Alfano, O. M. & Cassano, A. E. 2010 Decomposition of 2-chlorophenol employing goethite as Fenton catalyst. I. Proposal of a feasible, combined reaction scheme of heterogeneous and homogeneous reactions. *Appl. Catal. B Environ.* **95**(1–2), 1–13.

Ozisik, M. N. 1973 *Radiative Transfer and Interactions with Conduction and Convection*. J. Wiley, New York.

Pawliszyn, J. 1999 *Applications of Solid Phase Microextracción*. The Royal Society of Chemistry, UK.

Pignatello, J. J., Oliveros, E. & MacKay, A. 2006 Advanced oxidation processes for organic contaminant destruction based on the fenton reaction and related chemistry. *Crit. Rev. Environ. Sci. Technol.* **36**(1), 1–84.

Son, H. S., Im, J. K. & Zoh, K. D. 2009 A Fenton-like degradation mechanism for 1,4-dioxane using zero-valent iron (Fe0) and UV light. *Water Res.* **43**(5), 1457–1463.

Teel, A. L., Dennis, D. F., Jeremy, T. S., Lynn, M. C. & Richard, J. W. 2007 Rates of trace mineral-catalyzed decomposition of hydrogen peroxide. *J. Environ. Eng.* **133**(8), 853–858.

Toxicological Profile for Chlorophenols 1999 U.S. Department of Health and Human Services; Public Health Service Agency for Toxic Substances and Disease Registry, U.S. Government printing office: Washington, DC.

Yuranova, T., Enea, O., Mielczarski, E., Mielczarski, J., Albers, P. & Kiwi, J. 2004 Fenton immobilized photo-assisted catalysis through a Fe/C structured fabric. *Appl. Catal. B Environ.* **49**(1), 39–50.

Standard Methods for the Examination of Water and Wastewater 1995 19th edition, American Public Health Association, Washington, DC.

Zheng, Z. W., Lei, L. C., Xu, S. J. & Cen, P. L. 2004 Heterogeneous UV/Fenton catalytic degradation of wastewater containing phenol with Fe-Cu-Mn-Y catalyst. *J. Zhejiang Univ. Sci.* **5**(2), 206–211.